Astron. Astrophys. 325, 700–708 (1997)

ASTRONOMY
AND
ASTROPHYSICS

Quantitative spectroscopy of the He I cluster in the Galactic center⋆

F. Najarro[1], A. Krabbe[2], R. Genzel[2], D. Lutz[2], R.P. Kudritzki[1,3], and D.J. Hillier[4]

[1] Institut für Astronomie und Astrophysik der Universität München, Scheinerstr. 1, D-81679 München, Germany
[2] Max-Planck-Institut für extraterrestrische Physik, D-85740 Garching bei München, Germany
[3] Max-Planck-Institut für Astrophysik, D-85740 Garching bei München, Germany
[4] Department of Physics and Astronomy, University of Pittsburgh, 3941 O'Hara Street, Pittsburgh, PA 15260, USA

Received 7 January 1997 / Accepted 24 March 1997

Abstract. We present first results on quantitative infrared spectroscopy of the brightest He I emission line stars in the Galactic center. The observed He I and H broad emission lines are caused by extremely strong stellar winds ($\dot{M} \sim 5$ to 80 $\times 10^{-5}$ $M_\odot$ yr^{-1}) with relatively small outflow velocities ($V_\infty \sim$ 300 to 1000 km s^{-1}). The effective temperatures of the objects range from 17,000 K to 30,000 K with corresponding stellar luminosities of 1 to $30 \times 10^5 L_\odot$. Strongly enhanced helium abundances ($N_{He}/N_H > .5$) are found. These results indicate that the He I emission line stars are evolved blue supergiants close to the evolutionary stage of Wolf-Rayet stars. They power the central parsec and belong to a young stellar cluster of massive stars which formed a few million years ago.

Key words: stars: early-type – stars: mass-loss – stars: supergiants – stars: emission-line – Galaxy: center – infrared: stars

1. Introduction

The He I emission line cluster in the Galactic center discovered by Krabbe et al. (1991) provides a unique opportunity to test star formation and evolution in connection with the ionization and energetics of the Galactic center. Results of a detailed spectroscopic investigation of the brightest source (AF star) of the cluster in the He I 2.058μm line by Najarro et al. (1994) revealed that the AF star is a helium-rich blue supergiant/Wolf-Rayet star. It is characterized by a strong stellar wind and constitutes a moderate source of Lyman continuum photons. The latter result clearly suggested that the cluster of He I stars can make a significant contribution to the total luminosity and the Lyman continuum flux of the inner parsec. Therefore, it was crucial to analyze the spectra of other He I objects of the cluster and to obtain their stellar parameters to better constrain their role in the energetics of the central parsec. First results have been reported in Krabbe et al. (1995, hereafter Paper I) who concluded that there was a star formation burst centered about 7×10^6 years and with a significant (4×10^6 years) spread. Further, statistical evidence for a concentration of dark mass ($\sim 3\times10^6 M_\odot$) in the Galactic center was derived in Paper I from the stellar radial velocity dispersion. In this paper we concentrate on the detailed quantitative spectroscopic investigation of eight He I objects in the central parsec.

Send offprint requests to: F. Najarro

⋆ Based on observations collected at the European Southern Observatory at La Silla, Chile

2. Summary of observations

Spectroscopic observations of the He I cluster have been carried out using CSG4, FAST, SHARP and 3D, and are described in detail in Paper I.

Table 1 summarizes the observational results obtained for the He I objects analyzed in this work. Before using the above results as constraints to model the objects some remarks must be made concerning some of the observed values. From Table 1 we see that the extinction shows high variability on small spatial scales, and therefore individual estimates must be made for each object under consideration. For the wavelength range around the K-band we assume $A(K) = 1.53(A(H) - A(K))$ and $A(\lambda) = A(K)(\lambda/2.2\mu)^{-1.75}$ (Krabbe et al. 1995). The measured FWHM of the emission lines were used as an initial guess for V_∞, the terminal velocity of the stellar wind. The final V_∞ value was then obtained by fitting the computed profiles iteratively with those observed. Except for IRS 13E1, all He II 2.189μm line fluxes are upper limits. All available Pα fluxes were used as checks for the consistency of the results only, since the measurements suffer from a much higher uncertainty. Of concern is also the observed feature at $\lambda \approx 2.11\mu$m. Detailed inspection of the observed spectra indicates that the He I 2.112μm line contributes part, but not all by far of the observed feature. We clearly identify a broad blue component centered at $\lambda \approx 2.105\mu$m (i.e., $\sim$ 1000km s^{-1} bluewards from the He I 2.112μm triplet component) as well as a closer, overlapping red component ($\Delta V \approx$500km s^{-1}). Moreover, the individual spectra of some sources reveal the presence of a further redwards component at $\lambda \approx 2.121\mu$m ($\Delta V \approx$1400km s^{-1}).

Table 1. Observed properties for the brighter GC He I sources. All fluxes are dereddened and have been scaled to a distance of 1 kpc assuming a distance of 8.5 kpc to the Galactic center.

Star	A(H-K)	$F_{2.2\mu}$	$He\,I_{2.06}$	$B\gamma$	$P\alpha$	$He\,I_{2.112}$	$He\,II_{2.19}$	FWHM
				$He\,I_{7-4}$	$He\,I_{4-3}$	C III+N III		
		(Jy)		(10^{-10} erg s^{-1}		cm^{-2})		$km\,s^{-1}$
7W	2.7	20.1	5.56	1.10	<13	1.75	<.3	1000
13E1	2.7	139.	11.6	5.66	<50	8.47	∼.9	1000
16NE	2.0	125.	3.02	1.11	···	1.21	<.3	600
16NW	2.2	72.4	1.16	.421	···	.462	···	1000
16C	2.3	115.	2.69	.894	···	1.98	<.3	600
16SW	2.4	145.	5.04	2.09	···	2.02	<.5	650
15SW	2.3	66.3	7.53	1.04	<7	.909	···	850
15NE	2.3	46.3	6.27	1.30	<12	1.19	<.2	950

Table 2. He I, C III and N III line transitions around 2.11μm. Wavelengths are in air and velocity shifts are given relative to the He I 2.112μm line. The C III and N III (8-7) transitions are tabulated together as the differences between the transition wavelengths and oscillator strengths are negligible.

Transition	λ (μm)	Δ V($km\,s^{-1}$)
C III/N III $7g\,^2G - 8h\,^2H$	2.1032	−1250
C III $5s\,^1S - 5p\,^1P$	2.1075	−645
He I $3p\,^3P - 4s\,^3S$	2.1120	0
He I $3p\,^1P - 4s\,^1S$	2.1131	156
C III/N III $7h\,^2H - 8i\,^2I$	2.1146	364
C III/N III $7i\,^2I - 8k\,^2K$	2.1149	411
C III/N III $7i\,^2I - 8h\,^2H$	2.1150	419
C III $4p\,^1P - 4d\,^1D$	2.1217	1380

These features are likely to correspond to N III and/or C III lines. As a first approximation we may assume that the high lying levels of N III and C III can be treated as being hydrogenic. In this case, we obtain $\lambda \approx 2.116\mu$m for both the N III (8-7) and C III (8-7) transitions. The above estimate is rather crude, and does not explain the observed features. It is, therefore, necessary to resolve the n=7 and n=8 levels into their LS coupling terms, and consider the transitions among them separately together with their strengths. This has been done with the help of Keith Butler who kindly provided (private communication) the atomic data for the transitions of interest. These are presented in Table 2 which lists the strongest N III and C III transitions and their corresponding air wavelengths around $\lambda \approx 2.11\mu$m together with the He I lines.

As shown in Table 2 the differences between the N III and C III (8-7) transition wavelengths are negligible. Therefore, the observation of a well separated C III or N III line (e.g., C III 2.121μm see below) is required to establish whether the observed features are due to nitrogen and/or carbon. We see that N III and C III (8-7) essentially present two well separated components at λ=2.103μm and λ=2.115μm. The expected line strength ratio for the C/N 2.115 line to the C/N 2.103 lines is ≈4 and is consistent with higher S/N observations of other late type WN stars presented recently by Crowther & Smith (1996, see spectrum of WR105) and by Figer et al. (1995, star 1 in their paper). The C III 2.121μm line is well separated (ΔV≥1000 $km\,s^{-1}$) from the other lines. Hence, its contribution can be measured much more easily than that of the C III 2.108μm line (the latter is blended with both the C III/N III 2.103μm and He I 2.112μm lines), and may be used to determined which element is contributing to the 2.11μm feature.

It is readily apparent that the use of the He I 2.112μm line flux as an observational constraint to model the objects is far from ideal. Even in those cases where the spectral resolution achieved is sufficient ($\lambda/\Delta\lambda \geq 1500$) that the contribution of C III/N III 2.103μm, C III 2.108μm and C III 2.121μm can be removed, we cannot a priori distinguish which fraction of the remaining feature at λ=2.112μm is due to the C III/N III 2.115μm transitions. Hence, the measured line flux will give an upper limit for the true He I 2.112/3μm line. In other words, we obtain only an upper limit on the wind density, mass loss rate, in this fashion (e.g. Najarro 1995). Thus, the observed λ 2.112μm fluxes were considered as upper limits, and, if possible, the true He I 2.112μm line flux was estimated by subtracting a $\sim 2V_\infty$ wide region centered at 2.1120μm from the observed 2.11μm feature.

We find a clear qualitative resemblance of the He I stars spectra with that of the AF star (Najarro et al. 1994). There is, however, a substantial spread in the observed terminal velocities (500 – 1000$km\,s^{-1}$), line to continuum and line to line ratios. These differences reflect the different initial masses and evolutionary states of the objects. Below we report and discuss the main results from the modeling thus far obtained.

3. Model and first results

To model the objects we proceeded as in Najarro et al. (1994) and used the iterative, non-LTE method presented by Hillier (1987, 1990) which solves the radiative transfer equation in spherical geometry, subject to the constraints of statistical and radiative equilibrium, for the expanding atmospheres of early-type stars. We considered a pure H-He atmosphere with 12 H, 49 He I (n≤10) and 12 He II levels. The stellar parameters obtained for the above eight objects are presented in Table 3, while Table 4 displays the model line and continuum fluxes. Agreement

Table 3. Derived stellar parameters for GC He I sources. $R_{2/3}$ is the photospheric radius at Rosseland optical depth 2/3, $T_{2/3}$ the effective temperature derived for L_* and $R_{2/3}$ and $\eta = \dot{M}V_\infty/(L_*/c)$ is the "performance" number (Springmann 1994). Stellar parameters for the AF star (model A_{CG} in Najarro et al. 1994 are also displayed for comparison purposes.

	IRS Object								
	AF	16NE	16C	16SW	16NW	7W	13E1	15NE	15SW
R_* ($R_\odot$)	40	85	85	90	70	23	60	45	62
L_* ($10^5 L_\odot$)	2.00	22.0	19.0	25.9	10.3	4.10	22.6	9.10	10.5
$T_{\rm eff}$ (10^4K)	1.93	2.41	2.32	2.44	2.20	3.04	2.89	2.66	2.35
$R_{2/3}$ (R_*)	1.11	1.12	1.12	1.14	1.10	1.53	1.95	1.17	1.13
$T_{2/3}$ (10^4K)	1.83	2.27	2.20	2.29	1.77	2.46	2.07	2.46	2.20
He/H	1.7	1.0	3.0	1.3	1.3	>500	>500	>100	>100
$\dot{M}$ ($10^{-5} M_\odot$ yr^{-1})	8.7	9.50	10.5	15.5	5.30	20.7	79.1	18.0	16.5
V_∞ (km s^{-1})	700	550	650	650	750	1000	1000	750	700
η	15.	1.17	1.78	1.92	1.91	24.9	17.3	7.33	5.43
V_{rad} (km s^{-1})	200	-40	200	300	-100	-250	0	-150	-200
Log Q(H^+)	47	49.6	49.5	49.7	49.0	49.2	49.9	49.4	49.3
Log Q(He^+)	< 38	< 45	< 45	< 45	< 44	< 44	45.0	< 44	< 44
Log Q(He^{++})	< 30	< 32	< 32	< 32	< 31	< 33	< 33	< 33	< 32

Table 4. Computed continuum and line fluxes for the He I sources analyzed so far. All fluxes are given at 1 kpc.

Star	$F_{2.2\mu}$	He I$_{2.06}$	Bγ+He I$_{7-4}$	Pα+He I$_{4-3}$	He I$_{2.112}$	He II$_{2.19}$
	(Jy)		(10^{-10} erg s^{-1} cm^{-2})			
7W	20.3	5.64	1.09	7.5	.90	.05
13E1	139.	11.8	5.84	45.	5.30	.3
16NE	124.	3.06	1.75	20.	1.12	<.01
16NW	72.0	1.29	.46	7.0	.03	<.01
16C	114.	2.70	.85	11.0	.3	<.01
16SW	144.	5.15	2.40	26.	.60	<.01
15SW	66.1	6.62	1.02	9.2	.90	<.01
15NE	46.3	6.38	1.32	8.5	1.10	<.01

between observed and computed values was always better than 10%. Below we discus our results for the analyzed objects.

3.1. IRS 7W & IRS 13E1

IRS 7W is the hottest ($T_{\rm eff}\approx$30Kk) but also the least luminous (not considering the AF star) analyzed object of the new sample. Therefore, its stellar radius (R_*=23$R_\odot$) is smaller (by more than a factor of two) when compared with the other sources. The stellar parameters derived are similar to those of WN8 and WN9 stars (Hamann et al. 1993, Crowther et al. 1995a, 1996, Smith et al. 1995). Its observed near-IR spectrum clearly indicates a later spectral type than WN8 (Hillier 1985), and probably corresponds to a WN9 or WN10 type. Hydrogen is strongly depleted in IRS 7W, He/H$\geq$500 as found in some WNL stars (e.g., HD 177230, Conti & Massey 1989). It is important to note that the hydrogen abundance is strongly constrained by the absence of H Pα. This, together with the high degree of extension of the atmosphere $R_{2/3}/R_*>1.5$ and its high "performance" number ($\eta\approx$25, see Table 3) relate the object to WNE-w stars (Hamann et al. 1993), though the effective temperature of IRS 7W is low compared with other such stars.

IRS 7W and IRS 13E1 (see below) are the only He I objects in our sample for which the strongest optical He II lines are expected appear modestly in emission in the synthetic spectra. The equivalent width of He II 2.189μm from our models of IRS 7W is nevertheless too small to be detected, in agreement with the observations.

Fig. 1 shows the fits of our current best model for IRS 7W to the observed CGS4 He I 2.058μm, Bγ and He I 2.112μm profiles. The radial velocity was obtained by aligning the observed and computed profiles. We derived $V_{\rm rad}$=$-$250km s^{-1}. Diffuse He I and H emission has been removed from the observed profiles. The removal of the He I diffuse emission, though fainter and hence less problematic than that of H, significantly affects the resulting shape of the He I 2.058μm emission peak (see Fig. 1). The agreement of our model calculations with the observed He I 2.058μm line is excellent. It is also important to note that the strong emission component of the P Cygni profile significantly fills in the absorption dip.

The fit to the observed He I (7$-$4) lines confirms the absence of H in the atmosphere of IRS 7W. The centroid of the line is clearly displaced bluewards ($\Delta V\approx$300 km s^{-1}) from Bγ and the computed width of the He I (7$-$4) blend is fully consistent with the observations. The observed He I 2.112μm line profile also shows good agreement with the computed profile. The lack of an observed absorption dip is consistent with the previously mentioned presence of the blue N III/C III blend. The emission

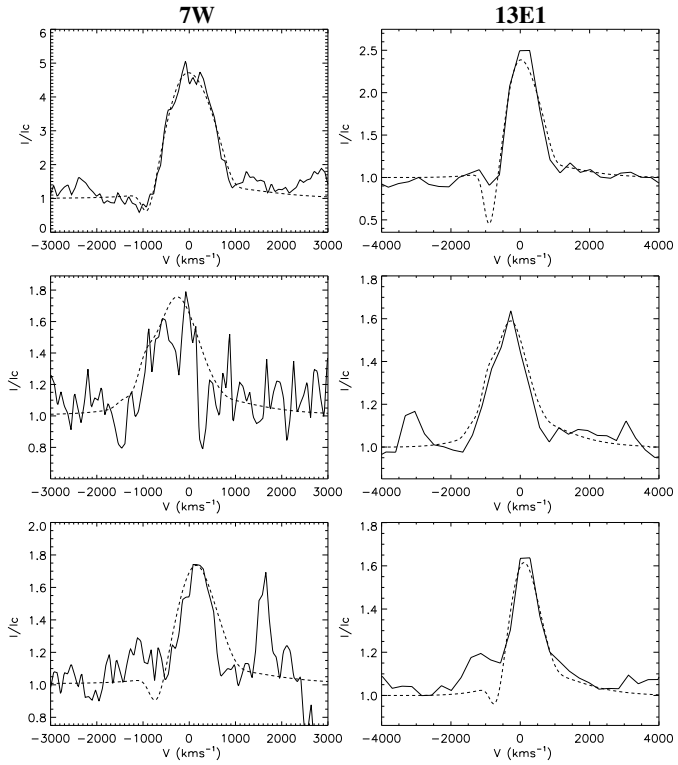

Fig. 1. left (from top to bottom): IRS 7W observed **CGS4** (solid) and computed (dashed) He I 2.058μm, Bγ and He I 2.112μm profiles. **right (from top to bottom)** IRS 13E1 observed **3D** (solid) and computed (dashed) He I 2.058μm, Bγ and He I 2.112μm profiles. Diffuse emission has been removed for both objects.

feature at ΔV$\approx$1400 km s^{-1}redwards of the He I 2.112μm line could be due in part to the C III 2.1217μm line, though the presence of interstellar S(1) could explain this feature as well. The latter seems a more plausible explanation as the observed feature is certainly narrower than the rest of the observed IRS 7W wind lines.

IRS 13E1 is also a rather hot source ($T_*\approx$29Kk) but because of its enormous degree of extension $R_{2/3}/R_*\approx2$, $V(R_{2/3})>V_\infty/3$, it presents a much lower $T_{2/3}$ value. This is essentially caused by the extremely high rate of mass-loss of the object ($\dot{M}\approx 8\times10^{-4}M_\odot$ yr^{-1}). Like IRS 7W, IRS 13E1 shows no stellar hydrogen features in its spectrum which confirms its highly evolved status, and hence it may be classified as a WN9 or WN10 star. Interestingly, its performance number ($\eta\approx17$) is slightly lower than that of IRS 7W, but still as high as those of WNE-w stars, and very similar to the values obtained for the AF star by Najarro et al. (1994, models A_{CG} and B_{CG}). Our models are able to reproduce the observed line and continuum fluxes reasonably well. The relatively high T_* and $\dot{M}$ are observationally supported by the presence of strong, extended ($\sim$2500 km s^{-1}) electron scattering wings. Only in the case of the He II 2.189μm line do we obtain a much weaker line flux (factor of 3) than observed, an inadequate result even if we consider the relatively high uncertainty (very low S/N) in the derivation of the He II 2.189μm line flux. We attribute our low computed He II 2.189μm line flux value to the neglect of line blanketing. The main effects of line blanketing (see for instance Hillier 1995) are a higher ionization degree in the inner regions of the atmosphere due to energy input by thermalization of the backscattered photons that hit the core (backwarming), and a lower ionization degree in the outer regions due to the increased opacity from the blocking lines (flux blocking). These effects should be enhanced for those stellar parameter domains in which the ionization degree of a major species is close to switching. Najarro (1995) has shown that this condition is met for He, and perhaps H, in the winds of most of the He I stars. Further, the higher the effective temperature of the object, the closer the shift of the He ionization degree from He II to He III. Therefore, we should expect line blanketing to critically affect the resulting He II 2.189μm line flux of the hotter objects, i.e., IRS 7W and IRS 13E1. Nevertheless, it is important to stress that the presence in emission of both the He I 2.058μm and He II 2.189μm lines constitutes an important constraint for the effective temperature of the object. If T_* is increased the He I 2.058μm line will rapidly come into absorption (e.g. Najarro et al. 1994), while a lower T_* value will dramatically decrease the amount of He III in the wind, and hence the equivalent width of the He II 2.189μm recombination line (see also Crowther et al. 1995b results for WR16). We estimate that both lines will appear in emission within an effective temperature range lower than 2000 K. A further important consequence of the observation of the He II 2.189μm line is that it requires the He I continuum to become optically thin (or at least be close) at the outer boundary, which means that the objects may become important sources of He I ionizing photons (see discussion in next section).

Our computed He I 2.058μm profile shows good general agreement with the observed **3D** one (see Fig. 1). The computed absorption dip is clearly deeper than that observed. This discrepancy may be due to clumping, stellar rotation and/or multiplicity of IRS 13E, as the high resolution narrowband He I images of Eckart et al. (1995) suggest the presence of at least one other weaker emission line star within $\approx1''$ of IRS 13E. It is important to note that the observed strong electron scattering wings are well reproduced by the computed profile. The contribution of the N III/C III (8-7) lines to the 2.11μm observed feature of IRS 13E1 is clearly shown in Fig. 1. Our computed He I 2.112μm profile, however, is able to reproduce the central part ($\pm V_\infty$) of the profile quite well. We see that due to the high wind density and relatively high V_∞value, the blue N III/C III 2.103μm component is blended with the He I 2.112μm line and fills in the P Cygni dip of the latter. Assuming that the blue feature is entirely due to N III/C III 2.103μm, we may conclude that we are severely overestimating the true contribution of the He I lines, since the red N III/C III 2.115μm component is expected to be more strongly in emission than the blue one. Therefore, both a higher spectral resolution and the inclusion of the N III and C III model atoms in our models are required to disentangle the 2.11μm puzzle.

The fit to the observed Bγ-He I (7−4) feature of IRS 13E1 is even more problematic. The Bγ line measured by **3D** is much stronger than the He I 2.058μm line, in contradiction to the ratio we have used to model the object, i.e., the results obtained from **FAST** and **CGS4** (line flux of He I 2.058μm≈2 that of Bγ). On the other hand, it is difficult to attribute a fraction of the observed **3D** Bγ line to a uniform diffuse contamination from the nebula, as **3D** obtains relatively "clean", diffuse emission free spectra. To complicate the picture even more, we note that IRS 13E appears to be embedded in a highly excited, ionized region (the wall of the "mini-cavity", see Genzel et al. 1994), and therefore the diffuse nebular emission from the surroundings is expected to be strong and probably not uniform (as confirmed by the **CGS4** results). Therefore, we have subtracted that fraction of the **3D** Bγ profile that we believe may be due to nebular emission, in order to obtain an observed profile consistent with other runs. The resulting diffuse subtracted Bγ-He I (7−4) profile is shown in Fig. 1 together with the fit from the model calculations. From Fig. 1 we see that the agreement between the observed and computed profiles is excellent. The observed profile has been redshifted by 50km s^{-1} and the shift is consistent with those applied to the He I 2.058μm and He I 2.112μm lines, 0 km s^{-1}.

The data set with the observed low resolution **CGS4** Bγ, Pα, He I 2.058μm and He I 2.112μm profiles (uncorrected for nebular emission) confirmed the strong contamination, even for He I, by diffuse nebular emission (see Najarro 1995). Therefore, no comparison can be made between the shape of the computed and observed raw **CGS4** hydrogen profiles (Bγ and Pα), until the observed data are further processed and the nebular emission is carefully removed (work in progress). Nevertheless, we note that the **CGS4** He I 2.058μm and He I 2.112μm lines show good agreement with the results obtained from the **3D**. The **CGS4** observations confirm the contribution of the N III/C III (8-7) lines to the 2.11μm feature, while the nebular emission seems to fill in the absorption dip of the He I 2.058μm line and enhance the observed peaks of both lines.

3.2. IRS 16 sources

The main and perhaps most interesting result from our analysis of the IRS 16 sources, i.e., IRS 16 NE, C, SW and NW, is that they show similar He/H ratios (He/H∼1, see Table 3). Since the values obtained for the stellar luminosities and effective temperatures of the objects are also very close (only IRS 16NW has a slightly lower L_* and $T_{\rm eff}$), we may conclude that the brighter IRS 16 sources have similar ages. This result is also supported by the almost identical values obtained for the performance numbers (see Table 3), since η constitutes a powerful indicator of the evolutionary status of the star (Lamers & Leitherer 1993).

The presence of hydrogen in the observed spectra is consistent with a WNL evolutionary phase, though the effective temperatures obtained for the IRS 16 objects is rather low when compared to the values derived for other later type (WN9-10) WNL stars (Crowther et al. 1995a). On the other hand, Smith et al. (1995) have recently obtained similar stellar parameters to our IRS 16 values for a WR star in M33 (MCA1-B) and a galactic WR star (WR105), which they classify as WN9 stars. However, these two objects clearly show He II 4686 in emission (EW∼10Å), while this line is almost absent in our models (EW≤.1Å). We attribute this discrepancy to the small but crucial difference between the derived effective temperatures (our $T_{\rm eff}$ values are ≈ 2000 K lower), which once more indicates the sensitivity of the He II and He I lines in this stellar parameter domain (see also Crowther et al. 1995a). From Table 3 we see that all IRS16 objects are important sources of Lyman continuum photons, while their contribution to the He I continuum is negligible.

Fig. 2 shows the excellent agreement between the observed **3D** and computed He I 2.058μm profiles for the IRS 16 sources. The obvious P Cygni shape of the observed profiles, confirms the wind nature of the lines. The average radial velocity derived from the fits to the He I 2.058μm, He I 2.112μm and Bγ lines are −40, 200, 300, and −100 km s^{-1} for IRS 16NE, C, SW and NW respectively. From the fits to the observed **3D** 2.11μm features we note that our results are able to reproduce the He I 2.112μm component quite well. Despite the relatively low S/N ratio, Fig. 2 confirms the presence of the N III/C III (8-7) lines in three of the IRS 16 sources (NE, C and SW), while they are much weaker in the spectrum of IRS 16NW (as confirmed by Genzel et al. 1996). This result is consistent with the lower temperature ($\Delta T_{\rm eff}$ ∼1500 K) and wind density obtained for the latter, as we expect the strength of the N III/C III (8-7) lines to decrease with decreasing T_* and wind density. This would also explain the absence of these features in the spectrum of the AF star (lower $T_{\rm eff}$) and their relatively large strength in the hotter, denser IRS 13E1 and IRS 7W.

General good agreement between the computed and observed **3D** Bγ-He I (7−4) lines is also found. The presence of a blue absorption dip in the observed IRS 16SW Bγ line may be attributed to the aforementioned problematic subtraction of the diffuse nebular emission. Though both the broadness of the observed Bγ-He I (7−4) profiles and the velocity corrections applied to them are consistent with the He/H ratio obtained from our models (see Fig. 2), they constitute a rather crude constraint for the accurate determination of the He/H ratio due to the small velocity separation of the He and H components. As for the AF star, Pα observations of the IRS 16 objects would provide the most direct test to confirm (or reject) the abundances obtained in our analysis. Unfortunately, this task was not feasible with **CGS4** due to the insufficient spatial resolution of the instrument for the crowded IRS 16 complex. Thus, future observations Pα with **3D** would provide definite constraints to the hydrogen content of these sources. If, on the other hand, the tiny blue absorption dips present in the Bγ-He I (7−4) profiles are real (see also Genzel et al. 1996) this would indicate a lower He abundance, what has already been found by Figer et al. (1996) for the LBV star in the quintuplet and Hillier et al. (in prep.) for the galactic LBV HDE316285.

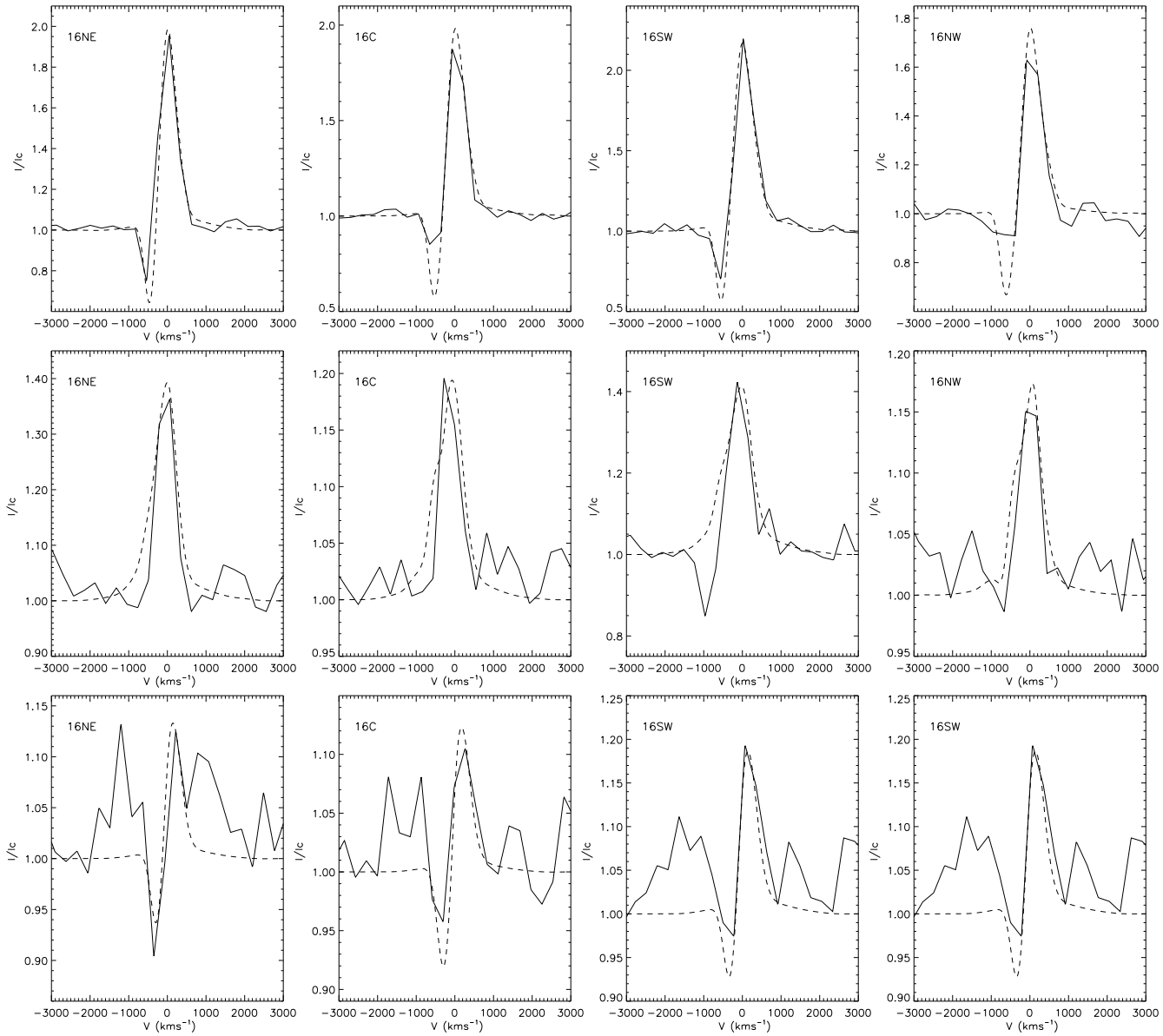

Fig. 2. Observed **3D** profiles for the IRS 16 sources compared with the calculations (He I 2.058μm, Bγ and He I 2.112μm from top to bottom). The presence of the weak absorption dips in the Bγ lines may be attributed to the problematic subtraction of the diffuse nebular emission

3.3. IRS 15SW & IRS 15NE

IRS15NE and IRS15SW may be considered as "transition" objects. These objects have effective temperatures only slightly higher ($T_{eff}\sim$25000 K) than those obtained for the IRS16 objects. However, they appear to be pure He sources (as do IRS7W and IRS13E1). A further indication for this "transition" status is given by the performance numbers and terminal velocities shown in Table 3.

Both IRS 15NE IRS 15SW have relatively "modest" stellar radii (R_*=45$R_\odot$ and R_*=62$R_\odot$respectively). These values yield stellar luminosities a bit lower ($L_*\sim 10^6 L_\odot$) than those of the IRS16 objects. However, due to the slightly higher effective temperature, both objects appear to be moderate sources of Lyman continuum photons ($\log Q(H^+) \approx 49.4$ each). As shown above, the stellar luminosity for the He I objects, and hence the number of Lyman continuum photons deposited in the interstellar medium is primarily set by the K-band continuum measurements. We are quite confident of the continuum measurements of IRS 15SW because the **SHARP** maps reveal it to be a fairly isolated source, while IRS 15NE appears as a multiple source (Eckart & Genzel priv. comm.). We measured K= 11.0 for the He I object. A direct comparison with the low resolution spectra obtained with **CGS4** is not possible because diffuse contamination dominates the observed spectrum and this contamination can only be poorly estimated and subtracted. We expect the reduced data from the **3D** campaign (work in progress), which has a higher spatial resolution, to provide stronger constraints

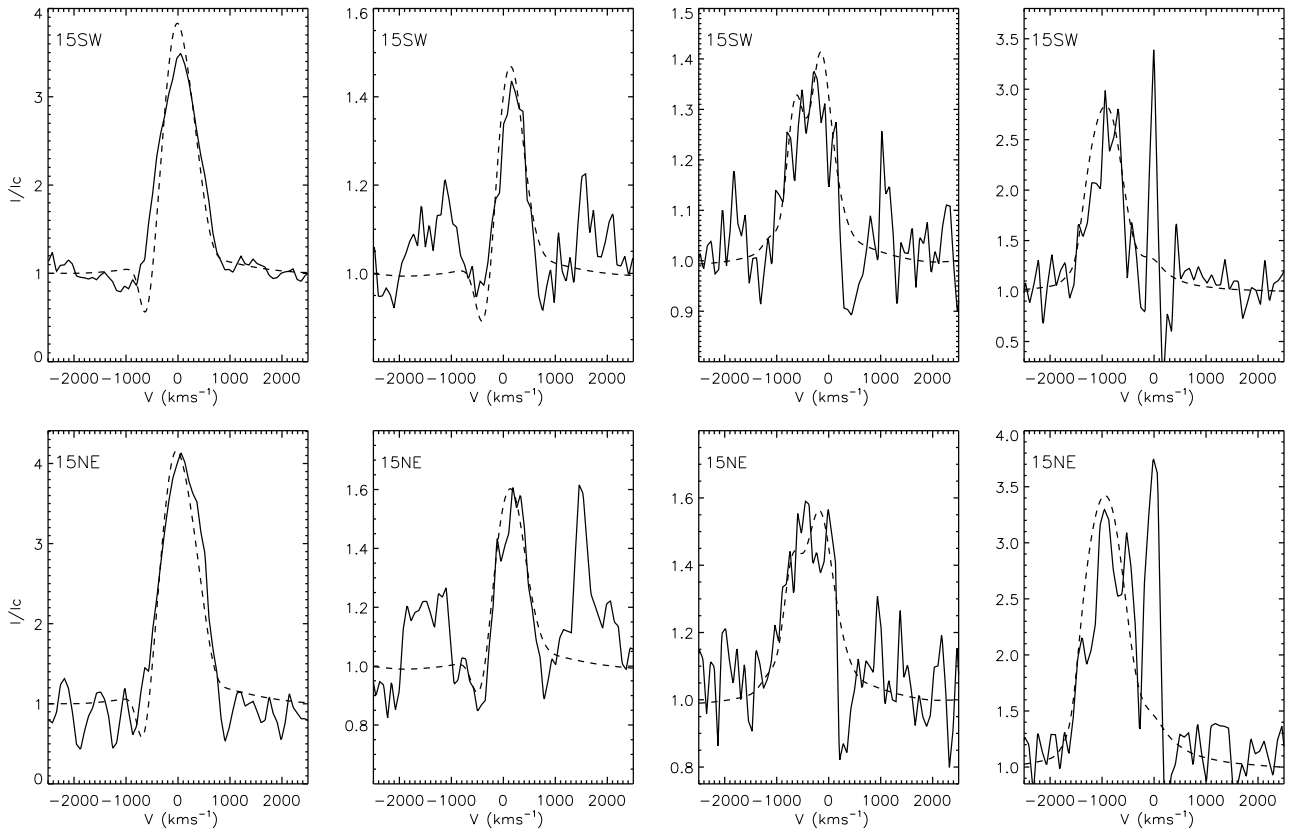

Fig. 3. IRS 15SW and IRS 15NE observed **CGS4** (solid) and computed (dashed) He I 2.058μm,He I 2.112μm,Bγ and Pα profiles. Most of the diffuse emission has been removed, though some narrow residual features have remained on the Pα profiles. The emission features bluewards and redwards the He I 2.112μm (see text and Table 2) may indicate an N and C enhancement. The velocity scale for Bγ and Pα is defined for the H component. The shift reflects the dominance of the He I component.

for these objects. Preliminary results from the **CGS4** data reduction are available for IRS 15SW and IRS 15NE profiles, and are compared below with our model calculations.

Fig. 3 shows the general good agreement of our model calculations with the observed IRS 15SW He I 2.058μm, He I 2.112μm, Bγ and Pα lines. The corresponding large slit width for the **CGS4** pixels (3.1$''$) hinders a clean subtraction of the relatively non-uniform background and diffuse emission, and therefore tends to blur the P Cygni dips of the He I lines (see Fig. 3). This effect is even more extreme for the H lines (see the Bγ and Pα lines in Fig. 3) where a "hole" or a narrow peaked feature at the wavelength of the hydrogen component may result from the presence of a non-uniform background. Despite these problems, our computed profiles are able to reproduce the shapes of the observed profiles satisfactorily (see Fig. 3). Further, the velocity displacements applied to all observed profiles are consistent ($\approx$200 km s^{-1}), and the broader blends for the observed He I (4$-$3) and He I (7$-$4) profiles are excellently matched by our computed profiles. We note, once more, the clear presence of the N III/C III 2.103μm feature bluewards of the He I 2.112μm line.

For IRS 15NE, our computed profiles fit the observed He I 2.058μm, He I 2.112μm, Bγ and Pα profiles reasonably well (see Fig. 3). As for IRS 16NE, the 2.11μm feature shows the presence of both the N III/C III 2.103μm component bluewards of the He I 2.112μm line, as well as the red N III/C III 2.115μm component, which clearly points to an enhanced abundance of these elements in the wind of IRS 15NE. Similarly to IRS 15SW the difficult background subtraction caused by the large slit width for the **CGS4** pixels blurs the P Cygni dips of the He I lines, while for Bγ and Pα a "hole" and/or a narrow peak feature appear at the wavelength of the hydrogen component due to the presence of non-uniform background and diffuse emission. Again, we expect the forthcoming **3D** results to provide less contaminated profiles which will better constrain the stellar parameters of these objects.

3.4. Evolutionary status, ionizing flux and GC mass

To gain further insight into the nature and evolutionary status of the He I emission line objects we show in Fig. 4 the positions of those analyzed in this work on the H-R diagram together with Schaller et al. (1992) evolutionary tracks for solar abundance. Of concern is the narrow $T_{\rm eff}$ band covered by these stars. As stated by Najarro et al. (1994) the identification of possible WN sources in the K-band is a difficult task due to the absence of

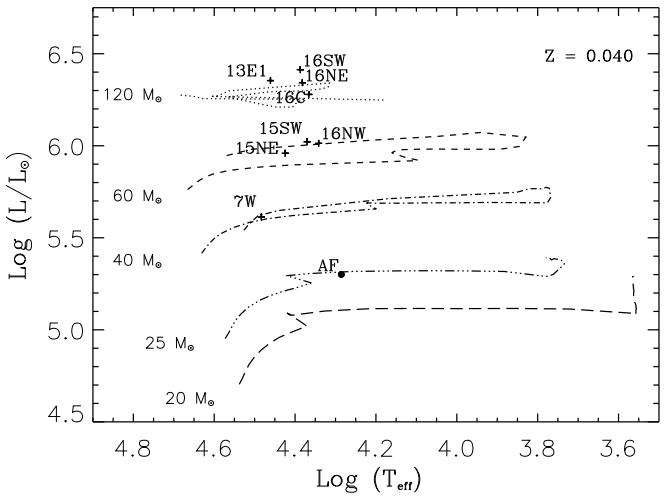

Fig. 4. Positions of the He I stars in the H-R diagram together with Schaller et al. (1992) evolutionary tracks for twice solar abundance.

strong nitrogen signatures in this spectral region (only the rather weak N III (8-7) and N III 5p-5s 2.247μm or N V (11-10) lines may be observed).

Nevertheless, as indicated above IRS13E1 and IRS7W fulfill many of the classical characteristics of WN9-WN10 stars, i.e., $T_{\rm eff}\approx$30 kK, depleted H, and high "performance" numbers $\eta \approx$ 17 for IRS13-E1 and $\eta \approx$ 25 for IRS7W. Moreover, IRS13E1 adds the presence of He II lines as a further WN feature.

The evolutionary status of IRS15NE and IRS15SW is somewhat problematic. Their composition, i.e., the absence of H, points towards a Wolf-Rayet phase for these objects. However, the other stellar parameters suggest a Ofpe/WN9 classification, the main caveat for a WN9 to WN11 classification being the low effective temperature. Recent work by Norbert Langer (personal communication) shows that the inclusion of pulsational instabilities in the evolutionary calculations of massive stars leads to a more efficient mixing, i.e., transport of He to the stellar surface, and hence a hydrogen deficient WNL stage may already be reached for relatively low effective temperatures after the red-turnover. This, in term, may explain the stellar parameters obtained for IRS15NE and IRS15SW.

We retain the Ofpe/WN9 classification for the IRS16 sources as their He content and effective temperarutre are close to that of the AF star and they show very similar stellar parameters to other known Ofpe/WN9 objects (Crowther et al. 1995a). However, except for the enhanced He content, the stellar parameters of the IRS16 sources (high R_*, L_* and $\dot{M}$ and low V_∞) also resemble those of some known LBVs such as P Cygni (e.g., Najarro 1995, Langer et al. 1994) or He 3-519 (Smith et al. 1994). This is confirmed by the recent K-Band spectra of the IRS16 sources obtained by Genzel et al. (1996, see Fig.1) which show remarkable similarities with those of other LBVs and P Cygni Type stars as LBV in the quintuplet (Figer et al. 1996), HDE316285 (Hillier et al. in prep.), the luminous companion of SGR 1806-20 (van Kerkwijk et al. 1995) or the G79 object (Waters, priv. comm.). Considering once more the effective mixing through pulsation instabilities, we may conclude that the IRS16 objects are just finishing their LBV phase. This result agrees with previous observational studies (Stahl et al. 1983, Walborn 1982, Wolf et al. 1988) in which a direct observational link between LBVs and Ofpe/WN9 stars was established.

In Paper I Krabbe et al. analyzed the nuclear star cluster using the star cluster models of Krabbe et al. (1994) and concluded that the observations fit a $7\pm1 \times 10^6$yrs old decaying burst in which $\sim$30000 stars formed very well. They obtain a model with a bolometric luminosity of L(Bol)$\sim 2.7 \times 10^7 L_\odot$ and a bolometric to Lyman luminosity ratio of ten. Such a model predicts 15 OB stars with L$\geq 3 \times 10^5 L_\odot$, 30 later type WR stars (WNL, WCL and the He I objects observed) and 2 to 4 KM supergiants with L(K)/L(Lyman)$\sim 3 \times 10^{-2}$. Further, the implied supernova rate (one in 4×10^4yrs) agrees with the interpretation of Sgr. A East (Genzel et al. 1994). Moreover, the presence of a fairly large number ($\sim$10) of moderately luminous late type stars in the central $8''$ also indicates (see Haller & Rieke 1989) an earlier starburst perhaps 10^8yrs ago. The above results clearly favor a model in which the central parsec of the Galaxy is powered by a cluster of hot stars, as earlier proposed by Rieke & Lebofsky (1982) and Allen & Sanders (1986). The eight objects studied here alone, already supply $\approx 3 \times 10^{50}$ Lyman continuum photons per second ($>$ 60% of the total Lyman flux as estimated from thermal radio continuum measurements by Genzel et al. 1994). Therefore, **the hot star cluster can fully account for the bolometric and Lyman ionizing luminosities of the central parsec**. None of these objects contribute to the He I-continuum. Even IRS13E1 does not provide more than 1% of the flux required for the He-ionization of the SgrA West HII region, $\log Q(\mathrm{He}^+) \approx 49$ (Krabbe et al. 1991). Hence, some hotter O and/or WR stars is required to account for the He I-continuum. The presence of the latter has been confirmed in Paper I, and recently by Genzel et al. (1996) In Paper I, two possible WC9 stars have been detected. For IRS16SE-1 and IRS16SE-2 strong broad emission at 2.11μm (possibly due to the contribution of two C III lines at 2.1081 and 2.117μm) was found as well as another set of possible C IV features at 2.07 and 2.08μm. Similar spectral characteristics have been found by Eenens et al. (1991) for the WC9 star WR88. The number of known WR in the central parsec has been recently increased with the detection of a WN8 and a WN5-6 star by Genzel et al. (1996). Also Blum et al. (1995) have recently detected a WC9 star at a 0.5pc projected radius ($14''$) from the Galactic center. The object is rather faint (K$\geq$12) and shows He I, C II and C IV lines in emission.

Finally, we may use the derived radial velocities to obtain the velocity dispersion of the objects and therefore, by means of the virial theorem (and/or the Bahcall-Tremaine estimator, Bahcall et al. (1981), derive the enclosed mass in the central parsec. In Paper I velocity measurements were obtained from Gaussian fits to the observed profiles for 35 early- and late-type stars. The radial velocity determinations from our quantitative analysis of Pα, He I 2.058μm, He I 2.112μm and Bγ lines confirm those obtained in Paper I. A mass concentration of $\sim$2 to $4\times10^6 M_\odot$was derived, thus finding a high statistical signif-

icance for a dark mass concentration. The latter could be in the form of massive stellar remnants ($10M_{\odot}$), i.e., the black hole cluster option suggested by Morris (1993), or more likely as a massive black hole (Genzel et al. 1994, Eckart & Genzel 1996a,1996b).

Acknowledgements. F. N. acknowledges a grant of the DARA under WE2- 50 OR 9413 6.

References

Allen D.A., Sanders R.H., 1986, NATURE, 319, 191
Bahcall J.N., Tremaine S., 1981, ApJ, 244, 805
Blum R.D., Sellgren K., DePoy D.L., 1995, ApJ, 440, L17
Conti P.S., Massey P., 1989, ApJ, 337, 251
Crowther P.A., Smith L.J., 1996, A&A, 305, 541
Crowther P.A., Hillier D.J., Smith L.J., 1995a, A&A, 293, 172
Crowther P.A., Hillier D.J., Smith L.J., 1995b, A&A, 293, 403
Eckart A., Genzel R., Hofmann R., Sams B.J., Tacconi-Garman L.E., 1995, ApJ, 445, L23
Eckart A., Genzel R., 1996a, NATURE, 383, 415
Eckart A., Genzel R., 1996b, MNRAS (in press)
Eenens R.P.J., Williams P.M., Wade R., 1991, MNRAS, 252, 300
Figer D., McLean I.S., Morris M., 1995, ApJ, 447, L29
Figer D., Najarro F., McLean I.S., Morris M., Geballe T.R., 1996, in "Luminous Blue Variables: Massive Stars in Transition", ed. A. Nota, Kona, Hawaii, (in press)
Genzel R., Hollenbach D.J., Townes C.H., 1994, Rep.Progr.Phys., 57, 417
Genzel R., Thatte N., Krabbe A., Kroker H., Tacconi-Garman L.E., 1996, ApJ, 472, 153
Haller J.W., Rieke M.J., 1989, in The Center of the Galaxy, ed. M.Morris, Kluwer, Dordrecht, 487
Hamann W.R., Koesterke L., Wessolowski U., 1993, A&A, 274, 397
Hillier D.J., 1985, AJ, 90, 1514
Hillier D.J., 1987, ApJSS, 63, 947
Hillier D.J., 1990, A&A, 231, 116
Hillier D.J., 1995, in: IAU Symp. 163, Wolf-Rayet Stars: Binaries, Colliding Winds, Evolution, eds. K. A. van der Hucht and P. M. Williams, Kluwer, Dordrecht, p. 116
Krabbe A., Genzel R., Drapatz S., Rotaciuc V., 1991, ApJ, 382, L19
Krabbe A., Stenberg A., Genzel R., 1994, ApJ, 424, 72
Krabbe A., Genzel R., Eckart A., et al., 1995, ApJ, 447, L95 (Paper I)
Lamers H.J.G.L.M. , Leitherer C., 1993, ApJ, 412, 771
Langer N., Hamann W.-R., Lennon M., et al., 1994, A&A, 290, 819
Morris M., 1993, ApJ, 408, 496
Najarro F., 1995, PhD Thesis, University of Munich
Najarro F., Hillier D.J., Kudritzki R.P., et al., 1994, A&A, 285, 573
Rieke G.H., Lebofsky M.J., 1982, in AIP Conference Proceedings 83: The Galactic center, eds. G. Riegler, R. Blandford, New York, 194
Schaller G., Schaerer D., Meynet G., Maeder A., 1992, A&AS, 96, 269
Smith L.J., Crowther P.A., Prinja R.K., 1994, A&A, 281, 833
Smith L.J., Crowther P.A., Willis A.J., 1995, A&A, 302, 830
Springmann U., 1994, A&A, 289, 505
Stahl O., Wolf B., Klare G., et al., 1983, A&A, 127, 49
van Kerkwijk M.H., Kulkarni S.R., Mathews K., Neugebauer G., 1995, ApJ, 444, L33
Walborn N.R., 1982, ApJ, 256, 452
Wolf B., Stahl O., Smolinski J., Cassatella A., 1988, A&A Suppl., 74, 239

This article was processed by the author using Springer-Verlag LaTeX A&A style file *L-AA* version 3.